Journal of
Instrumentation

Simulation and characterisation of a 16-by-96 multi-anode MCP-PMT for the TORCH detector

To cite this article: A. Abdelmotteleb *et al* 2026 *JINST* **21** C07011

Published by IOP Publishing for Sissa Medialab

Received: *March 17, 2026*
Accepted: *May 18, 2026*
Published: *July 10, 2026*

7[th] International Workshop on New Photon-Detector
Bologna, Italy
3–5 December 2025

Simulation and characterisation of a 16-by-96 multi-anode MCP-PMT for the TORCH detector

A. Abdelmotteleb,[l] M. Adinolfi,[g] M. Armour,[l] T. Blake,[k,l] T. Conneely,[c] D. Cussans,[g] A. Davidson,[l,*] S. Dekkers,[e] R. Dzhygadlo,[b] U. Egede,[e] T.C. Fearon,[g] C. Frei,[a] R. Forty,[a] R. Gao,[f] T. Gershon,[l] T. Gys,[a] T. Hadavizadeh,[e] G. Hallett,[l] N. Harnew,[f] D. Hu,[j] K. Jewkes,[l] S. Korpar,[d] M. Kreps,[l] J. Lapington,[i] M. Lehuraux,[l] P. Li,[h] J. Liu,[j] A. Lowe,[f] M. Loutit,[l] T. Ma,[j] I. Mackay,[f] S. Malde,[f] S. Mao,[h] A. Markfort,[c] J. Milnes,[c] A. Mitra,[l] R. Pestotnik,[d] D. Piedigrossi,[a] W. Qian,[h] R. Rabadan,[l] J. Rademacker,[g] G. Schepers,[b] J. Schwiening,[b] M. Shao,[j] T. Slater,[f] S. Stanislaus,[f] E. Walton,[e] N. Wang,[h] Y. Wang,[j] B. Westhenry,[g] G. Wilkinson,[f] A. York[f] and L. Zhu[h]

[a] *CERN, Geneva, Switzerland*
[b] *GSI Helmholtzzentrum für Schwerionenforschung GmbH, Darmstadt, Germany*
[c] *Photek Ltd, Saint Leonards-on-Sea, East Sussex, U.K.*
[d] *Experimental Particle Physics Department, Jožef Stefan Institute, Ljubljana, Slovenia*
[e] *School of Physics and Astronomy, Monash University, Melbourne, Australia*
[f] *Department of Physics, University of Oxford, Oxford, U.K.*
[g] *School of Physics, University of Bristol, Bristol, U.K.*
[h] *School of Physical Sciences, University of Chinese Academy of Sciences, Beijing, China*
[i] *School of Physics and Astronomy, University of Leicester, Leicester, U.K.*
[j] *School of Physics, University of Science and Technology of China, Hefei, China*
[k] *Department of Physics and Astronomy, University of Victoria, Victoria, Canada*
[l] *Department of Physics, University of Warwick, Coventry, U.K.*

E-mail: alex.davidson@warwick.ac.uk

Abstract: Owing to their single-photon sensitivity and fast rise time, micro-channel-plate photomultipliers (MCP-PMTs) make good candidates as photon detectors for the Time Of Internally Reflected CHerenkov light detector (TORCH) that is proposed as part of the phase two upgrade of the LHCb experiment. The TORCH detector has a target time resolution per photon of approximately 70 ps, required to achieve an approximately three standard deviation separation of pions and kaons at 10 GeV/c from their time-of-flight over a 10 m flight distance. A new high-granularity 16-by-96

[*] Corresponding author.

https://doi.org/10.1088/1748-0221/21/07/C07011

2026 JINST 21 C07011

channel MCP-PMT with a directly coupled anode has been developed in conjunction with Photek Ltd. This device is designed to decrease the pixel pitch to 0.55 mm in the fine pixel direction, giving improved spatial resolution and importantly lower per-pixel occupancies. This paper will cover cross-talk characterisation studies, used to determine the spatial resolution of the device. The experimental results are compared with simulation studies. Overall, the results demonstrate minimal effects of cross-talk on the device's output. A study of a TORCH demonstrator, using older 8-by-64 channel MCP-PMTs, has also been carried out in a beam test at CERN. Initial results from the demonstrator show suitable mechanical and optical performances.

Keywords: Detector modelling and simulations II (electric fields, charge transport, multiplication and induction, pulse formation, electron emission, etc); Secondary electron emitters and dynodes and their production; Photon detectors for UV, visible and IR photons (vacuum); Cherenkov detectors

2026 JINST 21 C07011

Contents

1 TORCH detector concept

The Time Of Internally Reflected CHerenkov radiation (TORCH) detector is designed to enhance the particle-identification capabilities of the LHCb detector at the LHC [1]. The nominal detector design features an array of 18 modules comprising a 66-by-250-by-1 cm^3 fused-silica radiator. Particles traversing the fused-silica radiators produce Cherenkov photons that are propagated to the periphery of the detector via total-internal-reflection, where they are focused by cylindrical focusing optics onto an array of fast-timing photon detectors. By accurately reconstructing the photon path in the detector, the photon arrival time can be used to separate different types of charged-hadrons by their time-of-flight over the 9.5 m distance from the interaction region to TORCH. To obtain the desired π–K separation at 10 GeV/c momentum, individual photons must be timed to 70 ps to achieve a 15 ps per-particle resolution when averaged over the $\sim$ 30 photons detected for each particle.

Two photon-detector technologies have been explored for TORCH, micro-channel-plate photo-mulitpliers (MCP-PMTs) and silicon photomultipliers (SiPMs). Both technologies face challenges in the environment expected during the high-luminosity phase of the LHC. Micro-channel-plate PMTs offer excellent time resolution but are limited by their lifetime and rate-capabilities (for a review see refs. [2, 3]). Silicon photo-multipliers will likely need to be cryogenically cooled to achieve manageable dark count rates after being subjected to large neutron fluence ($> 10^{12}$ 1 MeV neutron equivalent per cm^2 [4]). The large detector occupancy expected in the most central modules also places stringent requirements on the granularity of the photon detectors. These proceedings describe the development of MCP-PMTs for the project in conjunction with Photek Ltd.

2 TORCH demonstrator

A full-sized TORCH module was constructed in 2025 for use in beam tests with a mixed π/p charged-particle beam at the CERN PS to demonstrate the viability of the TORCH concept. The full-sized radiator was formed from three pieces of fused-silica (one of 125-by-66-by-1 cm^3 and two of 67.5-by-66-by-1 cm^3) that were bonded with a structural adhesive. The radiator is supported by a light-weight carbon-fiber structure designed to minimise the amount of material inside the acceptance of the LHCb detector. The structure is supported by rails in a light-tight enclosure. For the final experiment it is envisaged that the enclosure will be replaced by thin carbon-fiber panels.

The demonstrator uses six square 5.3-by-5.3 cm^2 MCP-PMTs developed as part of a R&D programme with Photek Ltd [5]. Eleven MCP-PMTs would be required to cover the full width of the

2026 JINST 21 C07011

module. The MCP-PMTs have a fused-silica input window with a S20 multi-alkali photocathode. They have 64-by-64 pads that are electronically ganged to form 8-by-64 pixels with a capacitively-coupled anode that is connected to an external PCB using anisotropic conductive film. The capacitive coupling leads to signals that are spread over 2–4 pixels for gain in the range of 1–2 million photoelectrons. Charge-sharing, and charge-centroiding in the reconstruction, is exploited to achieve an effective granularity of about 8-by-128. Atomic layer deposition (ALD) is used to achieve a lifetime in excess of $5\,C/cm^2$ [6]. The electronics for the prototype [7] are based on the NINO [8] and HPTDC [9] ASICs developed originally for the ALICE experiment, with the HPTDC operated with 100 ps TDC binning and the system read out via gigabit Ethernet. For the final project, electronics based on the FastRICH ASIC [10] are envisaged.

The MCP-PMTs have been extensively tested in laboratory measurements to measure their properties (gain, quantum efficiency and time response). The MCP-PMTs and electronics have also been previously tested with a half-scale demonstrator, where the time response of the full system has been shown to be compatible with the needs of the project [11]. Analysis of data collected with the full-sized demonstrator is ongoing. To achieve the required time-response the electronics are calibrated to account for time-walk in the NINO and integral-non-linearity in the HPTDC. A dedicated charge-injection system has been developed to improve the electronics calibration for the 2025 beam test analysis. The focus of the initial analysis has been on understanding the impact of the module assembly and the glue joints on the photon yield. First results from the demonstrator are discussed in ref. [12] and show that a high-quality optical connection has been achieved.

3 Development of a 16-by-96 multianode MCP-PMT

The capacitive coupling scheme of the 8-by-64 pixel device results in very large per-pixel occupancies in the environment expected for TORCH. To reduce the expected occupancy, a new device has been developed with Photek that replaces the capacitive coupling with direct coupling via vias. For this to be successful the image point-spread and cross-talk between pixels must be controlled to confine the signal to 1–2 pixels. It is also necessary to increase the granularity of the anode to compensate for the loss in spatial precision without charge-centroiding. A new ceramic anode with 16-by-96 pixels is specifically designed to achieve these requirements. This granularity results in a very dense arrangement of channels on the back of the device, given that each pixel must be read out individually. Individual channels are connected via 110 pin Hirose FX25 connectors, with one in every eight pins of the connector grounded. To reduce heating of the indium vacuum seal, laser soldering is used to connect the connectors to the anode. The device tested in these proceedings has only every other connector connected, and without the complication of close-packed connectors, achieved a connectivity of $> 95\%$. The first attempt to instrument a complete device only achieved an electrical connectivity at the level of about 70%. The low success rate may have been due to excessive cooling of the tube, reducing heat to the solder balls, or due to a misalignment of the solder mask. Optimisation of the soldering process is ongoing to achieve better connectivity.

The microchannel-plate configuration of the device is conventional, with two lead-glass plates arranged in a Chevron configuration. Each plate has a thickness of 700 µm and 15 µm pores that are separated by a 19 µm spacing. The resistivity of the plates is chosen to try to maximise the current that can be sustained by the MCP-PMT. The pores have an 8 degree bias angle and are coated with an aluminum oxide emissive layer that is deposited by ALD. The top and bottom of

2026 JINST 21 C07011

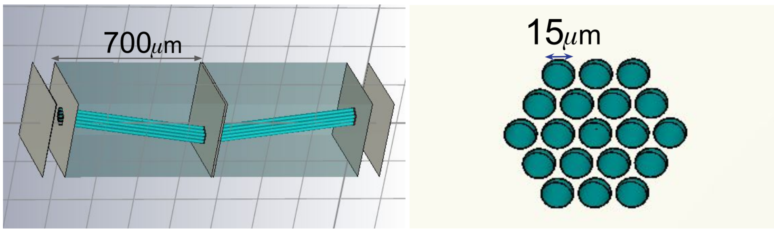

Figure 1. Microchannel-plate geometry in the device simulation. The blue region indicates the aluminum-oxide coating of MCP pores and the red region their Nichrome end-spoiling. The planes represent measurement positions in the simulation.

each pore has a Nichrome end-spoiling region. Multilayer (e.g. the Photonis R2D2 treatment) ALD treatments could eventually be used to extend the lifetime of the device beyond $30\,\mathrm{C/cm^2}$ [13] but have not been used with this prototype.

Potential differences are applied between the photocathode and top of the MCP stack ($V_c - V_{in}$), across the full MCP-stack ($V_{in} - V_{out}$) and between the output of the MCP and the anode ($V_{out} - V_a$). No potential difference is applied between the two MCPs.

3.1 Simulation of the 16-by-96 multianode MCP-PMT

To understand the expected device performance, the MCP-PMT is simulated in a three stage process. First, an electrostatic simulation of the electric field in the device is performed using Dassault Systèmes CST studio stationary-current solver. Second, a particle-in-cell simulation of the transport and avalanche gain of the electrons within the MCP stack that includes space-charge effects is performed in CST studio. Finally, a SPICE model [14] of the anode is used to evaluate the charge seen on different readout pins. This model includes the capacitance effects of the anode's internal routing, via a capacitance matrix generated by electrostatic modeling. To reduce the complexity of the models meshing, a region of around 40 pores is considered. An example of a simulated geometry is shown in figure 1.

As has been noted in previous studies, material properties have a significant impact on the predicted gain at a given value of the voltage difference between V_{in} and V_{out}. The avalanche gain process is parameterised according to ref. [15], with the material secondary electron yield (SEY) tuned to match ref. [16] (with a maximum of 2.7 electrons at an incident energy of 284 eV). This is also found to reproduce the typical gain seen in real 8-by-64 like devices, see figure 2. Large variations in gain are seen between different devices operated at the same $V_{in} - V_{out}$. These variations are likely due to variations in the thickness of the ALD coating, variations in the flatness of the MCPs and variations in the pore bias angle. The simulation is therefore not used as a quantitative comparison for any individual device but instead used to qualitatively understand their performance. Figure 3(left) shows the waveform the induced signal at the back of the device resulting from the avalanche gain process in the 16-by-96 device. Good control over the image-spread is seen, with a low level of charge-sharing between neighbouring pixels.

3.2 Measurements with the 16-by-96 multianode MCP-PMT

To understand the performance of the real detector, measurements have been made using a 407 nm picosecond-pulsed light-source that is focused to a $< 10\,\mu\mathrm{m}$ spot-size and scanned across the surface of

2026 JINST 21 C07011

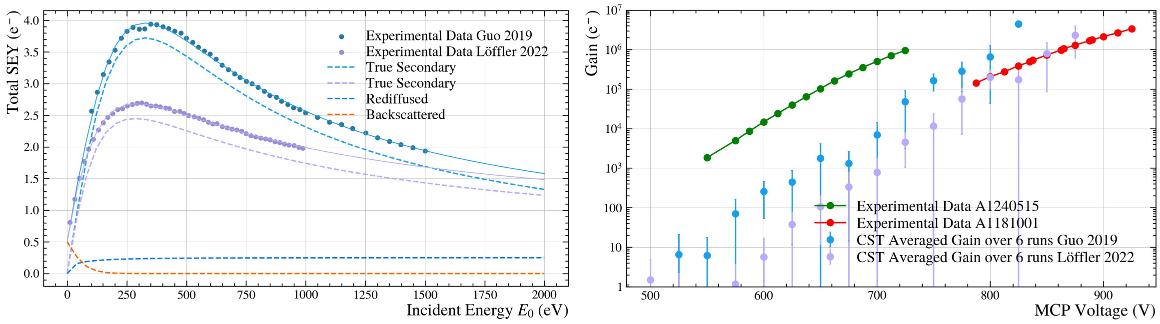

Figure 2. Secondary electron yield (SEY) as a function of incident electron energy (left) and gain as a function of the voltage across each MCP (right). Two different SEY behaviors are used, corresponding to refs. [17] and [16].

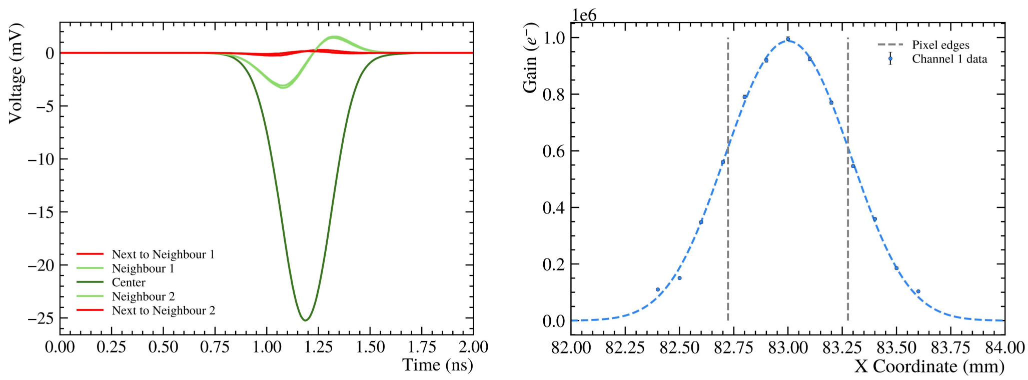

Figure 3. Waveform of the induced voltage over a 50 Ω terminating resistor from a SPICE model of the 16-by-96 pixel anode resulting from the simulated signal and capacitance matrix (left) and gain as function of position of the light source as seen by one detector channel (right). The vertical lines indicate the size of the pixel.

the device in 100 µm steps. A breakout board is used to read the signal from a set of four neighbouring pins to a Lecroy waveMaster 808zi-A (8 GHz, 40 GS/s) oscilloscope. Figure 3(right) shows the gain seen on an individual pixel as a function of the laser position. The gain value is obtained by fitting a model (a Polya function) to the charge distribution seen over a large number of laser triggers. The resulting image has a FWHM of ∼ 500 µm, which is comparable to the pixel size in the fine-pixel direction, demonstrating that a small image spread is obtained. If the laser is centred on a pixel, the signal in neighbouring pixels is measured to be 13% of that of the central pixel. For comparison, the simulation obtains a slightly smaller integrated-charge ratio of 6%. Work is ongoing to understand the source of this difference. Figure 4 shows the uniformity of the photocathode process obtained by illuminating different regions of the device. A good quantum uniformity is achieved over the illuminated region, with a photocurrent that is stable within ±5%. The transit-time spread of the device is measured using a laser splitter and a reference photodiode to be 40 ps [18], which is consistent with the time resolution requirements of TORCH.

2026 JINST 21 C07011

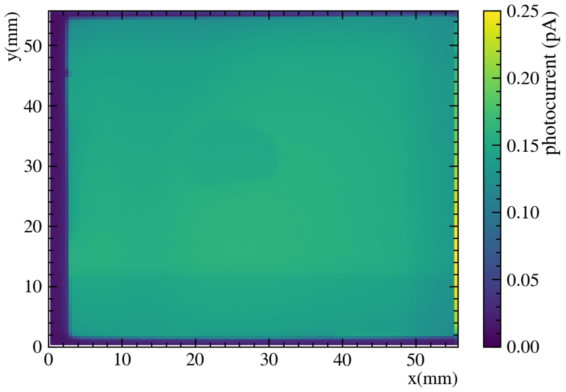

Figure 4. Uniformity of the quantum efficiency of the prototype 16-by-96 device, obtained using a picoameter and a focused laser source scanned over the device on a grid with a 250 µm spacing.

Acknowledgments

The authors would like to thank the Science and Technologies Facilities Council and UKRI for supporting this project through their industrial Cooperative Awards in Science and Technology scheme.

References

[1] LHCb collaboration, *Framework TDR for the LHCb Upgrade II: Opportunities in flavour physics, and beyond, in the HL-LHC era*, CERN-LHCC-2021-012 (2021).

[2] T. Iijima, *Status and perspectives of vacuum-based photon detectors*, *Nucl. Instrum. Meth. A* **639** (2011) 137.

[3] T. Gys, *Micro-channel plates and vacuum detectors*, *Nucl. Instrum. Meth. A* **787** (2015) 254.

[4] A. Ciccotelli et al., *Energy deposition studies for the Upgrade II of LHCb at the CERN Large Hadron Collider*, *Phys. Rev. Accel. Beams* **27** (2024) 061003 [`arXiv:2310.08281`].

[5] T.M. Conneely et al., *The TORCH PMT: a close packing, multi-anode, long life MCP-PMT for Cherenkov applications*, 2015 *JINST* **10** C05003.

[6] T.M. Conneely, J.S. Milnes and J. Howorth, *Extended lifetime MCP-PMTs: Characterisation and lifetime measurements of ALD coated microchannel plates, in a sealed photomultiplier tube*, *Nucl. Instrum. Meth. A* **732** (2013) 388.

[7] R. Gao et al., *A precision time of flight readout system for the TORCH prototype detector*, 2022 *JINST* **17** C05015.

[8] F. Anghinolfi et al., *NINO: An ultra-fast and low-power front-end amplifier/discriminator ASIC designed for the multigap resistive plate chamber*, *Nucl. Instrum. Meth. A* **533** (2004) 183.

[9] M. Mota et al., *A flexible multi-channel high-resolution time-to-digital converter ASIC*, in the proceedings of the *2000 IEEE Nuclear Science Symposium. Conference Record (Cat. No.00CH37149)*, Lyon, France (2000) [`DOI:10.1109/nssmic.2000.949889`].

[10] LHCb RICH collaboration, *The FastRICH ASIC for the LHCb RICH enhancements*, *Nucl. Instrum. Meth. A* **1067** (2024) 169664.

[11] S. Bhasin et al., *Performance of a prototype TORCH time-of-flight detector*, *Nucl. Instrum. Meth. A* **1050** (2023) 168181 [`arXiv:2209.13379`].

2026 JINST 21 C07011

[12] A. Abdelmotteleb et al., *Design, assembly and beam validation of a full-scale TORCH module*, *Nucl. Instrum. Meth. A* **1089** (2026) 171542.

[13] A. Lehmann et al., *Systematic approach to measure the performance of microchannel-plate photomultipliers*, *Nucl. Instrum. Meth. A* **1065** (2024) 169536 [arXiv:2403.13938].

[14] M.T. Engelhardt, *SPICE Differentiation*, *LT Journal of Analog Innovation* (2015).

[15] M.A. Furman and M.T.F. Pivi, *Probabilistic model for the simulation of secondary electron emission*, *Phys. Rev. ST Accel. Beams* **5** (2002) 124404 [*Erratum ibid.* **16** (2013) 069901].

[16] J. Löffler et al., *A comprehensive analysis of electron emission from a-Si:H/Al_2O_3 at low energies*, *J. Phys. D* **56** (2023) 065306.

[17] J. Guo et al., *Secondary electron emission characteristics of Al_2O_3 coatings prepared by atomic layer deposition*, *AIP Adv.* **9** (2019) 095303.

[18] A. Davidson et al., *Next generation microchannel plate detectors for high spatial and temporal resolution*, 2025 *JINST* **20** C06018.